JCI The Journal of Clinical Investigation

# PRICKLE3 linked to ATPase biogenesis manifested Leber's hereditary optic neuropathy

Jialing Yu, … , Pingping Jiang, Min-Xin Guan

*J Clin Invest.* 2020. https://doi.org/10.1172/JCI134965.

Research In-Press Preview Genetics Ophthalmology

## Graphical abstract

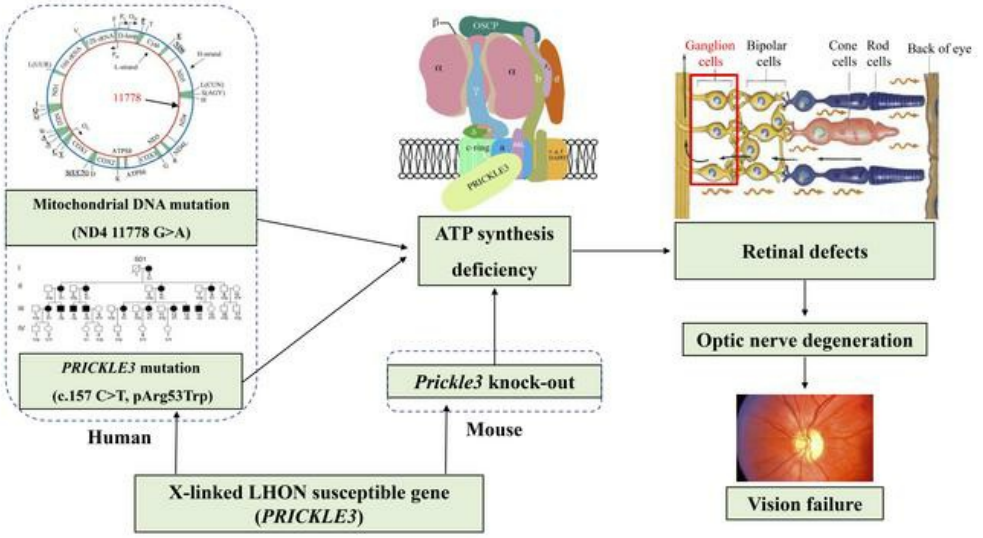


**Find the latest version:**

https://jci.me/134965/pdf

**PRICKLE3 linked to ATPase biogenesis manifested Leber's hereditary optic neuropathy**

Jialing Yu[1,2,3#], Xiaoyang Liang[2#], Yanchun Ji[1,2#], Cheng Ai[2#], Junxia Liu[2], Ling Zhu[1,2], Zhipeng Nie[2], Xiaofen Jin[2,3], Chenghui Wang[2], Juanjuan Zhang[2,4], Fuxin Zhao[4], Shuang Mei[2], Xiaoxu Zhao[1,2], Xiangtian Zhou[4], Minglian Zhang[5], Meng Wang[1,2], Taosheng Huang[6], Pingping Jiang[1,2]* and Min-Xin Guan[1,2,3,7]*

[1]The Children's Hospital, Division of Medical Genetics and Genomics, Zhejiang University School of Medicine and National Clinical Research Center for Child Health, Hangzhou, Zhejiang, China

[2]Institute of Genetics and Department of Human Genetics, Zhejiang University School of Medicine, Hangzhou, Zhejiang, China.

[3]Key Laboratory of Reproductive Genetics, Ministry of Education of PRC, Hangzhou, Zhejiang, China

[4]School of Optometry and Ophthalmology and Eye Hospital, Wenzhou Medical University, Wenzhou, Zhejiang, China

[5]Department of Ophthalmology, Hebei Provincial Eye Hospital, Xingtai, Hebei, China

[6]Division of Human Genetics, Cincinnati Children's Hospital Medical Center, Cincinnati, Ohio, USA

[7]Joint Institute of Genetics and Genomic Medicine between Zhejiang University and University of Toronto, Zhejiang University, Hangzhou, Zhejiang, China

#The first four authors have equally contributed to the work.

*Corresponding authors: Min-Xin Guan, Ph.D., Institute of Genetics, Zhejiang University School of Medicine, 866 Yuhangtang Road, Hangzhou, Zhejiang 310058, China; Tel: 86-571-88206916; Fax: 86-571-88982377; E-mail: gminxin88@zju.edu.cn;

Pingping Jiang, Ph.D., Department of Human Genetics, Zhejiang University School of Medicine, 866 Yuhangtang Road, Hangzhou, Zhejiang 310058, China; Tel: 86-571-88208328; Fax: 86-571-88982356; E-mail: ppjiang@zju.edu.cn.

**Conflict of interest**

The authors declare that no conflict of interest exists.

**Abstract**

Leber's hereditary optic neuropathy (LHON) is a maternally inherited eye disease. X-linked nuclear modifiers were proposed to modify the phenotypic manifestation of LHON-associated mitochondrial DNA (mtDNA) mutations. By whole exome sequencing, we identified the X-linked LHON modifier (c.157C>T, p. Arg53Trp) in the *PRICKLE3* encoding a mitochondrial protein linked to biogenesis of ATPase in three Chinese families. All affected individuals carried both ND4 11778G>A and p.Arg53Trp mutations, while subjects bearing only single mutation exhibited normal vision. The cells carrying the p.Arg53Trp mutation exhibited the defective assembly, stability and function of ATP synthase, verified by *PRICKLE3* knock-down cells. Co-immunoprecipitation indicated the direct interaction of PRICKLE3 with ATP synthase via ATP8. Strikingly, mutant cells bearing both p.Arg53Trp and m.11778G>A mutations displayed greater mitochondrial dysfunctions than those carrying only single mutation. These indicated that the p.Arg53Trp mutation acted in synergy with m.11778G>A mutation and deteriorated mitochondrial dysfunctions necessary for the expression of LHON. Furthermore, we demonstrated that *Prickle3* deficient mice exhibited the pronounced ATPase deficiencies. *Prickle3* knock-out mice recapitulated LHON phenotypes with retina deficiencies including degeneration of retinal ganglion cells and abnormal vasculature. Our findings provided new insights into pathophysiology of LHON that were manifested by interaction between mtDNA mutation and X-linked nuclear modifier.

**Key words:** Mitochondrial DNA mutation, optic neuropathy, X-linked nuclear modifier, ATPase biogenesis, pathophysiology.

## Introduction

Leber's hereditary optic neuropathy is the most common maternally inherited eye disease (1). This disorder is characterized by bilateral, painless, subacute, central visual loss in young adults (2,3). The typical features in this disorder included the primary degeneration of retinal ganglion cells (RGCs) and accompanied by ascending optic atrophy (4,5). Mutations in mitochondrial DNA (mtDNA) have been identified to contribute to the pathogenesis of LHON though to varying degrees (6-10). Of these, the m.11778G>A mutation in ND4 gene encoding a subunit of NADH:ubiquinone oxidoreductase (complex I) is the most prevalent LHON-associated mtDNA mutation worldwide (7-12). However, only relatively mild mitochondrial dysfunctions, especially the reduced activity of complex I, were observed in mutant cells carrying the m.11778G>A mutation (13-16). There were marked variations in the penetrance and gender bias occurred in the LHON pedigrees carrying the mtDNA mutation, reflecting the complex etiology of this disease (1,5,17,18). Our recent study demonstrated that several LHON families were manifested by synergic interaction between m.11778G>A mutation and mutated autosomal recessive modifier *YARS2* encoding mitochondrial tyrosyl-tRNA synthetase (15). The incomplete penetrance and gender bias in patients presenting with optic neuropathy suggests an X-linked modifier gene necessary for the phenotypic expression of LHON-associated mtDNA mutations (19). Despite statistical support for the linkages of several putative nuclear modifier loci in X chromosome, the exact gene has yet to be identified (20-21).

In this study, we performed the whole-exome sequencing of genetically

uncharacterized patients with LHON by taking advantage of a large cohort of 1281 Chinese probands with LHON (11,22,23). As a result, we identified a novel LHON susceptibility allele (c.157C>T, p. Arg53Trp) in the *PRICKLE3* at the Xp11.23, which located at the putative nuclear modifier loci for the phenotypic expression of LHON-associated mtDNA mutations (20,21). The *PRICKLE3* encodes a highly conserved protein enriched in mitochondria, whose *Drosophila* and *Xenopus* homologues are involved in the planar cell polarity and vision function (24-26). We then performed Sanger sequence analysis of symptomatic and asymptomatic individuals among 211 Chinese and 58 Caucasian pedigrees carrying m.11778G>A mutation and 1515 Chinese and 237 Caucasian control subjects lacking the m.11778G>A mutation. Functional significance of the *PRICKLE3* mutation was assessed through use of lymphoblastoid mutant cell lines derived from matrilineal relatives of Chinese families (individuals carrying only the m.11778G>A mutation, or both m.11778G>A and heterozygous or hemizygous *PRICKLE3* mutations), normal vision individuals carrying only *PRICKLE3* mutation and genetically unrelated control subjects lacking these mutations. The effect of p.Arg53Trp mutation on oxidative phosphorylation system (OXPHOS) was further evaluated for the activity and assembly of mitochondrial ATPase using the *PRICKLE3* knockdown in HeLa cell by shRNA. To investigate whether defects in *PRICKLE3* cause the degeneration of retinal ganglion cells *in vivo*, we studied the *Prickle3* knock-out mice produced by genome editing using the CRISPR/Cas9 system.

## RESULTS

### Identification of *PRICKLE3* mutation by whole exome sequencing

We performed the whole exome sequencing of DNA from four members (proband III-14, affected mother II-8 and unaffected sibling III-15 and father II-7) of SD1 family carrying the m.11778G>A mutation (Figure 1A and Supplemental Table 1) (27). The overview of the exome analysis was summarized in Supplemental Figure 1 and Table 2. After removing annotated polymorphisms and filtered for variants, a single exonic variant (c.157C>T) (Chr. X: 49040342 C>G, hg 19) in the exon 3 of *PRICKLE3* gene was identified at the Xp11.23, which localized at the putative modifier region predicted to manifest the phenotypic expression of LHON (20,21). The c.157C>T mutation changed a highly conserved 53 arginine with tryptophan (p.Arg53Trp) at the N-terminal of the PRICKLE3 (Figure 1B). PRICKLE3 is a highly conserved protein from vertebrate to primates (Supplemental Figure 2), belonging to the PRICKLE family involved in planar cell polarity necessary for the development of retina (26,28).

We then carried out the Sanger sequence analysis of DNA fragments spanning all exons and their flanking sequences of *PRICKLE3* among 35 members of this family (Supplemental Table 3). Of 21 matrilineal relatives, 5 symptomatic males carried the hemizygous c.157C>T mutation, 9 symptomatic females harbored the heterozygous c.157C>T mutation, and 7 (4 females and 3 males) asymptomatic subjects lacked the c.157C>T mutation. No other sequence changes were detected among these individuals. Of other family members lacking the m.11778G>A mutation, only one female subject

(IV-3) carried the heterozygous c.157C>T mutation, remaining individuals lacked the c.157C>T mutation. We further analyzed the presence of c.157C>T mutation in 345 symptomatic and 234 asymptomatic subjects from 210 Han Chinese pedigrees, 58 symptomatic and 58 asymptomatic subjects from 58 Caucasian pedigrees carrying m.11778G>A mutation, and 1515 (815 males and 700 females) Han Chinese and 237 (137 males and 100 females) Caucasian control subjects lacking the m.11778G>A mutation. Four male and 5 female symptomatic subjects belonging to pedigrees XT and AH harbored the hemizygous or heterozygous c.157C>T mutation, respectively. The c.157C>T mutation was absent among 234 Chinese asymptomatic subjects and 116 Caucasian subjects bearing the m.11778G>A mutation and 237 controls. The c.157C>T mutation was only present in hemizygous form in two males (XT-II-3, AH-I-1) and heterozygous form in one female (XT-III-6) married-in control subjects lacking the m.11778G>A mutation among 1515 Chinese control subjects. Furthermore, none of other functionally significant mtDNA variants was found in these families, suggesting that mtDNA backgrounds may not play an important role in the phenotypic manifestation of m.11778G>A mutation (Supplemental Table 4) (29). The co-segregation of LHON phenotype with the presence of both m.11778G>A and c.157C>T mutations in 9 males and 14 females suggested that the c.157C>T mutation is a rare X-linked dominant LHON susceptible allele.

**The p.Arg53Trp mutation affected the stability but not mitochondrial localization of PRICKLE3**

To investigate the effect of the p.Arg53Trp mutation on PRICKLE3, we examined the level of PRICKLE3 protein by Western blot analysis using mutant and control lymphoblastoid cell lines derived from members of SD1 pedigree. As illustrated in Figure 1*C*, the cell lines carrying the p.Arg53Trp mutation, together with or without m.11778G>A mutation, exhibited ~55% reductions in the levels of PRICKLE3 and no effect on the expression levels of PRICKLE1 and PRICKLE4, indicating a deleterious effect of p.Arg53Trp mutation on PRICKLE3 structure/function.

Potential mitochondrial dysfunction caused by the p.Arg53Trp mutation led to us to examine whether PRICKLE3 localizes at mitochondria. The Mitoprot program predicted that PRICKEL3 has a 0.3314 probability to entry into mitochondria with a 15 amino acid sequence targeting to mitochondria (30). To determine the mitochondrial localization of PRICKLE3, a HA-tagged version of PRICKLE3 was transiently expressed with in the HeLa cells. Cellular fraction experiments of HeLa cells revealed that the exogenous PRICKLE3 is enriched within mitochondrial fractions, along with outer mitochondrial membrane protein TOM20 and inner mitochondrial membrane protein ATP5F, and also present in cytosol, along with cytosolic protein Tubulin (Figure 1D). This indicates that mitochondria contain the PRICKLE3 protein. Furthermore, a light band of PRICKLE3 in isolated mitochondria was resistant to the treatment of Proteinase K, implying that PRICKLE3 may be recruited to the inner membrane for interaction or binding with protein(s) that anchored in the inner membrane. Moreover, a carboxy terminus HA-tagged wild type or mutant PRICKLE3

displayed the overlap with mitochondrial protein UQCRC2, with a significant correlation (pearson's coefficient of 0.61 and 0.55 for WT and MT, respectively) between red and green channels (Figure 1E). These results indicated that the PRICKLE3 localized to mitochondria, but the p.Arg53Trp mutation did not affect its mitochondrial location.

**The *PRICKLE3* mutation caused the defects of mitochondrial complex V function**

To evaluate the effect of the p.Arg53Trp mutation on the oxidative phosphorylation, we measured the activities of respiratory complexes from cell lines derived from subjects carrying only m.11778G>A, or p.Arg53Trp mutation, and both m.11778G>A with heterozygous or hemizygous p.Arg53Trp mutations. As shown in Figure 2*A*, the activity of complex I in the mutant cell lines carrying only m.11778G>A mutation, only p.Arg53Trp mutation, both m.11778G>A and heterozygous or hemizygous p.Arg53Trp mutations were 77%, 94%, 65% and 62% of the average values in control cell lines lacking these mutations, respectively. However, the activities of complex II, III and IV in all mutant cell lines were comparable with those of control cell lines. These suggested that the m.111778G>A mutation contributed to the reduced activity of complex I but the p.Arg53Trp mutation did not affect the activities of those complexes (Figure 2A). Strikingly, the activity of complex V in the mutant cell carrying only m.11778G>A mutation, only p.Arg53Trp mutation, both m.11778G>A and heterozygous or hemizygous p.Arg53Trp mutations were 87%, 56%, 49% and 32% of average values in control cell lines, respectively. The reduced activities of complex V in various mutant

cells were further confirmed by clear native polyacrylamide gel electrophoresis, supplied with mitochondrial ATPase substrates, reflecting 82%, 51%, 45% and 41% of average values in controls (Figure 2B) (31,32). Moreover, an F1 signal was markedly reduced among the different mutant cell lines. These data revealed that the p.Arg53Trp altered the activity of complex V but did not perturb the activities of other respiratory chain complexes.

To validate if the defective complex V activity caused by the p.Arg53Trp mutation, we measured the oxygen consumption rates (OCR) in various mutant and control cell lines. As shown in Figure 2C, mutant cell lines carrying only p.Arg53Trp or m.11778G>A mutation displayed mild reductions in the basal OCR and ATP-linked OCR, while more drastic reductions in these OCRs were observed in mutant cell lines carrying both m.11778G>A and p.Arg53Trp mutation. However, the *PRICKLE3* mutation did not affect the levels of 6 subunits of OXPHOS: NDUFA9, NDUFB8, SDHA, UQCRC2, CO2 and ATP5A (Supplemental Figure 3). To investigate if the mitochondrial contents reflect these biochemical data, we analyzed the mtDNA copy numbers in the mutant and control cell lines. No significant differences in the contents of mtDNA were detected among mutant and control cell lines (Supplemental Figure 4). Using luciferin/luciferase assay for measurement of ATP production, 53% reductions in the level in the mitochondrial ATP were observed in mutant cell lines carrying both m.11778G>A and p.Arg53Trp mutation, while only 28.6% and 40.7% decreases in the level in the mitochondrial ATP were observed in the cell lines carrying only

m.11778G>A or p.Arg53Trp mutation, respectively (Figure 2D). These suggested that the p.Arg53Trp mutation worsened the complex V deficiency caused by m.11778G>A mutation. However, the p.Arg53Trp mutation did not affect the levels of reactive oxygen species and mitochondrial membrane potentials (Supplemental Figure 5).

**The *PRICKLE3* mutation altered the stability of complex V**

To investigate whether the deficient ATP production results from the altered assembly or instability of mitochondrial ATP synthase, which consists of $F_0$ (c-ring and a, b, d, e, f, g, A6L subunits） and $F_1$ (α, β, γ, δ, ε subunits) regions (33,34). Mitochondrial membrane proteins from mutant and control cell lines were separated by blue native polyacrylamide gel electrophoresis and hybridized with ATP5A antibody (a nuclear encoded complex V subunit) and VDAC as the loading control. As illustrated in Figure 3A, the levels of complex V monomer in mutant cell lines carrying only m.11778G>A mutation, only p.Arg53Trp mutation, both m.11778G>A and heterozygous or hemizygous p.Arg53Trp mutations were 95%, 58%, 55% and 59% of mean values in control cell lines, respectively. These results were validated by approximately 31% decrease of fully assembled complex V observed in the PRICKLE3-silencing Hela cells and rescued by overexpression of PRICKLE3 (Figure 3B, Supplemental Figure 6). We then measured the levels of ATP6 (a), ATP8 (A6L), ATP5F(b), ATP5A (α), ATP5B (β), ATP5C (γ), subunits of ATP synthase and ATPAF1 involved in complex V assembly among mutant and control cell lines. Strikingly, the levels of ATP6, ATP8, ATPAF1 and ATP5B were markedly decreased in mutant cell lines carrying the

p.Arg53Trp mutation, while there were no significant differences in the levels of other subunits between mutant and control cell lines (Figure 3C). In fact, ATPAF1 binds specifically to ATP5B (β) as an assembly factor for $F_1$ (35), and ATP8 binds with ATP6 as a stator for the assembly of peripheral stalk and $F_1$ module (36, 37). This implicated the possibility of specific effect caused by the PRICKLE3 defect on the assembly of F1.

To examine if PRICKLE3 directly interacts with mitochondrial ATP synthase, we performed the immunoprecipitation assay using ATP Synthase Immunocapture Kit and HA antibody in mitochondria of HEK293T cell lines overexpressed with wild type and mutated forms of HA-tagged PRICKLE3. As shown in Figure 3D, PRICKLE3 and ATP Synthase or ATP8 (A6L) reciprocally immunoprecipitated, respectively. By contrast, PRICKLE3 did not precipitate ATP5A (α), ATP5B (β), ATP5F (b), ATPAF1, nor UQCRC2, respectively. These data demonstrated the interaction of PRICKLE3 with ATPase by specifically binding to the ATP8 (A6L) (Figure 3E).

***Prickle3* knock-out mouse exhibited the deficient function of complex V**

To investigate whether defects in PRICKLE3 cause the dysfunction of visual systems *in vivo*, we studied the *Prickle3* knock-out (KO) mice produced by the CRISPR/Cas9 system (Figure 4A, Supplemental Figure 7A). This deletion caused a frameshift resulting in a truncated Prickle3 protein with 61 amino acids (p.E61*) (Figure 4A). Both Western blot and immunohistochemistry data showed that Prickle3 was markedly reduced in the retina of *Prickle3* KO mice (Figure 4B and C). All *Prickle3*$^{+/-}$, *Prickle3*$^{-}$

$^{/0}$ and *Prickle3*$^{-/-}$ mice were viable. Moreover, *Prickle3* ubiquitously expressed in various layers of retina and other mice tissues (Supplemental Figure 7B). We then tested if the deletion of *Prickle3* caused mitochondrial dysfunction *in vivo*. The Prickle3 indeed localizes at mitochondria of in mouse embryonic fibroblast cells (Supplemental Figure 7C). The enzymatic assays revealed 52% and 67% decreases in the activities of complex V in the retina of *Prickle3*$^{+/-}$ and *Prickle3*$^{-/0}$/*Prickle3*$^{-/-}$ mice, respectively (Figure 4D). The reduced activities of ATP synthase in the *Prickle3*$^{-/0}$, *Prickle3*$^{-/-}$and *Prickle3*$^{+/-}$ mice were further confirmed by blue native polyacrylamide gel electrophoresis (Figure 4E). The altered assembly of complex V caused by deletion of *Prickle3* was evidenced by the 59% and 79% decrease of fully assembled ATP synthase in the *Prickle3*$^{+/-}$, *Prickle3*$^{-/0}$/ *Prickle3*$^{-/-}$ mice, as compared with WT mice, respectively (Figure 4F). Furthermore, *Prickle3* KO mice exhibited the various decreases in the levels of ATP8, ATP6 and ATP5B, as compared with those in the WT mice (Figure 4G). Moreover, the retina of *Prickle3*$^{+/-}$ and *Prickle3*$^{-/-}$ mice exhibited abnormal mitochondrial morphology including vacuolated, fragmented mitochondria and the loss of cristae (Figure 4H). These demonstrated that the deletion of *Prickle3* altered the function of mitochondrial ATPase. We concluded that the *Prickle3* KO mice recapitulated the biochemical phenotypes in the LHON patients.

***Prickle3* knock-out mouse exhibited the retinal defects**

We then investigated whether the loss of *Prickle3* led to the typical phenotypes of LHON including the degeneration of RGCs and vascular abnormalities. Retinal

functions from *Prickle3*$^{-/-}$, *Prickle3*$^{-/0}$, *Prickle3*$^{+/-}$and WT mice were first assessed by full-field electroretinography (ffERG), which measures widespread alteration of the functional integrity of the outer layer of the retina including photoreceptors and bipolar cells (38). The *Prickle3*$^{-/-}$, *Prickle3*$^{-/0}$ and *Prickle3*$^{+/-}$mice developed the retinal deficiency at the 4 weeks old.

Hematoxylin & eosin-stained retinal sections showed that the deletion of *Prickle3* did not change the thickness of layers in retina of mice (8 weeks) but caused the degeneration of RGCs (Figure 5A). To test if the deletion of *Prickle3* resulted in the loss of RGCs, the RGC layers from KO and WT mice were immune-stained with Brn3A, *β*-3-tubulin antibodies and DAPI to nuclei (39, 40). Especially, the RGC cells (Brn3a positive staining) in the retina ganglion layers of *Prickle3*$^{+/-}$ and *Prickle3*$^{-/-}$ mice reduced 22% and 39%, as compared with WT littermates, respectively (Figure 5B). These results demonstrated that the ablation of Prickle3 caused the loss of RGCs.

To assess if the deletion of *Prickle3* altered the function of RGCs, we examined the neurofilament network and RGC dendrites on the retina by whole retinal flat-mount staining using neurofilament heavy (NF-H) (neurofilament marker) antibody (41). Both *Prickle3*$^{+/-}$ and *Prickle3*$^{-/-}$mice exhibited much less neurofilaments in retina than those in WT mice (Figure 5*C*). These results suggested that the loss of Prickle3 altered the ramification of RGCs. To test if Prickle3 deficiency caused the RGC dendropathy, we measured the body areas and dendritic areas of one hundred NF-H positive cells. As shown in Figure 5D, the average total dendritic areas on RGCs in *Prickle3*$^{+/-}$ and

*Prickle3*$^{-/-}$ mice were 38%, and 66% of those in WT mice, respectively. By contrast, the body areas of RGCs in *Prickle3*$^{+/-}$ and *Prickle3*$^{-/-}$ mice were comparable with those in WT mice. The RGC dendritic pruning was further confirmed by Western blot analysis using the Psd95 (a postsynaptic protein) antibody (42). As shown in Figure 5E, Psd95 levels of retina in the *Prickle3*$^{+/-}$ and *Prickle3*$^{-/-}$ mice were 72% and 47% of those in the WT mice, respectively.

To examine if the mutant mice exhibited vascular abnormalities in the retina as LHON patients (44,45), we analyzed the retinal vasculature in in *Prickle3*$^{+/-}$, *Prickle3*$^{-/-}$ and WT mice at age of 8 weeks by labeling retina with isolectin B4 (a marker for vasculature) (43). As shown in Figure 5F, the vasculature in the *Prickle3*$^{+/-}$ and *Prickle3*$^{-/-}$ retina were tortuous and dilated, more branches in vessels, as compared with those in WT mice. Fluorescein angiography showed that no signs of fluorescein leakage in both eyes (Figure 5G), in a good agreement with pathological changes seen in LHON patients (44, 45). These data demonstrated that the *Prickle3* KO mouse recapitulated the typical features of clinical phenotypes in patients.

Retinal functions in the *Prickle3*$^{-/-}$, *Prickle3*$^{-/0}$, *Prickle3*$^{+/-}$ and WT mice were assessed by ffERG, focusing on photoreceptor deficits. As shown in Figure 5H, the amplitude of b-wave for scotopic (rod) responses, photopic (cone) responses and maximal combined rod-cone responses of *Prickle3*$^{+/-}$ , *Prickle3*$^{-/-}$ and *Prickle3*$^{-/0}$ mice eyes at age of 8 weeks were significantly declined, ranging from 24% to 34%, as compared with WT mice. These results suggested that the photoreceptor deficits or the

ERG phenotypes were the specific manifestations of RGCs, caused by the deletion of *Prickle3*.

**DISCUSSION**

The X-linked nuclear modifier genes were proposed to increase the penetrance and expressivity of optic atrophy in the LHON families carrying the mtDNA mutations (19-21). Using the whole exome sequence approach, in combination with functional assays and animal disease model, we identified the first X-linked LHON susceptibility allele (c.157C>T, p.Arg53Trp) in the *PRICKLE3* gene encoding a highly conserved mitochondrial protein for the phenotypic expression of the m.11778G>A mutation in three Chinese families. The *PRICKLE3* locates at the Xp11.23, which was the putative modifier locus to modulate the phenotypic expression of LHON (20, 21). Here, we demonstrated that the LHON phenotype was manifested by both m.11778G>A mutation and PRICKLE3 p.Arg53Trp mutation in hemizygosity in 9 males and heterozygosity in 14 females of 36 matrilineal relatives among these Chinese families. However, 2 male and 2 female subjects carrying only hemizygous or heterozygous p.Arg53Trp mutation did not develop the LHON phenotype, suggesting that the p.Arg53Trp mutation was by itself insufficient to produce a clinical phenotype, as in the case of YARS2 p.Gly191Val mutation (15). Furthermore, the homozygous p.Arg53Trp mutation was not detected in any female subjects carrying the m.11778G>A mutation in these Chinese and Caucasian families. Strikingly, three Chinese families bearing both m.11778G>A and p.Arg53Trp mutations exhibited much

higher penetrance (66%) and younger age-at-onset (16 years) of optic neuropathy than those in families harboring only a LHON-associated mtDNA mutations (8,9,10,11,17,18,46). In these Chinese families, there were no significant difference of average age-at-onset of LHON between male and female matrilineal relatives, while the affected females exhibited relatively more severe vision impairment than those affected males. Therefore, our data strongly suggested that the *PRICKLE3* mutation acted as an X-linked dominant susceptible allele increasing the penetrance and expressivity of LHON-associated mtDNA mutation. These were further supported by ~50% decrease in the levels of PRICKLE3 in mutant cell lines bearing either heterozygous or hemizygous PRICKLE3 mutation. However, this p.Arg53Trp mutation is a rare variant responsible for only a very small fraction of the male preponderance observed in LHON patients overall.

In this study, we demonstrated that the PRICKLE3 protein is directly linked to the biogenesis of the ATP synthase by specifically binding to the ATP8 (A6L) subunit. Human ATP synthase/complex V consists of $F_o$ and $F_1$ domains, connected by two stalks (36, 37). The $F_1$ domain is composed of subunits α, β, γ, δ, and ε, encoded by *ATP5A*, *ATP5B*, *ATP5C*, *ATP5D* and *ATP5E*, respectively, while $F_0$ domain consists of 8 subunits and transmembrane ring, including ATP6 and ATP8 (33,34). The biogenesis of complex V requires several proteins involved in $F_1$ and $F_0$ assemblies, including ATPAF1, ATPAF2 and TMEM70 (47-49). In this study, mutant cell lines carrying the p. Arg53Trp mutation exhibited marked decreases in the levels of ATP6, ATP8,

ATPAF1 and ATP5B. In fact, ATPAF1 bound specifically to ATP5B (β) as an assembly factor for $F_1$ (35), and ATP8 bound with ATP6 as a stator for the assembly of peripheral stalk and $F_1$ module (36, 37). Here, PRICKLE3 and ATP8 (A6L) reciprocally immunoprecipitated, suggesting the interaction of PRICKLE3 with ATPase by specifically binding to the ATP8 (A6L). Therefore, the p.Arg53Trp mutation may alter assembling and stabilizing ATP synthase and finally lead to ATP synthase deficiency. In this study, mutant cell lines bearing the p.Arg53Trp mutation or PRICKLE3-silencing Hela cells exhibited the significant decreases in the activity and specific contents of ATP synthase. In particular, the p.Arg53Trp mutation alone conferred ~40% reductions in the levels of mitochondrial ATP, as in the cases of cells carrying the *ATPAF2* and *TMEM70* mutations (50, 51). However, this reduced level of mitochondrial ATP in mutant cell lines carrying only p.Arg53Trp mutation is above a proposed threshold level, which is 50% of control levels in the mitochondrial ATP, to develop a clinical phenotype (52,53), indicating that the deficient ATP production by p.Arg53Trp mutation was by itself insufficient to produce the LHON phenotype. In the present study,~51% decreases in the mitochondrial ATP production in the mutant cell lines derived from affected matrilineal relatives resulted from the combination of defective ATPase activity caused by the p.Arg53Trp mutation with the m.11778G>A mutation-induced complex I deficiency. Strikingly, ~50% reductions of PRICKLE3 were correlated with 50% reductions in the ATPase activities in mutant cell lines bearing heterozygous or hemizygous PRICKLE3 mutation. These strongly suggested

that the PRICKLE3 p.Arg53Trp mutation is a haploinsufficient mutation which acted in synergy with m.11778G>A mutation and then deteriorated the mitochondrial dysfunctions necessary for the expression of LHON (54).

The lack of LHON-associated ND4 mutation animal model makes us difficult to elucidate the pathogenic mechanism underlying the interaction between the ND4 and Prickle3 mutations manifests the optic neuropathy *in vivo*. Therefore, we investigated biochemical and pathological consequences of *Prickle3* defects in retina using the *Prickle3* knock-out mouse. The *Prickle3* KO mice recapitulated the biochemical phenotypes in LHON patients. In particular, the pronounced deficiencies of ATPase observed in *Prickle3* KO mice were consistent with those in patients cell lines carrying both p.Arg53Trp and m.11778G>A mutations. In contrast with the moderate ATPase deficiency in human cell lines carrying only p.Arg53Trp mutation, the pronounced decreases in the ATPase activity caused by the deletion of *Prickle3* are likely sufficient to produce the LHON-like phenotype, including the degeneration of retinal ganglion cells, abnormal vasculature and optic nerve dysfunction (3,4,55,56). The *Prickle3* KO mice exhibited the significant decreases in RGC cells in retina ganglion layers, as in the case of the loss of RGC cells in the *Nduf4* KO mice (57). Strikingly, much less neurofilaments in retina of *Prickle3* KO mice than those in WT littermates implied the altered ramification of RGCs. These Prickle3-deficieny-indced defects in the planar cell polarity of RGCs were a good agreement with the known functions of Prickle family proteins (24,25,26,58). Furthermore, *Prickle3* KO mice exhibited the RGC dendropathy,

as evidenced by marked reductions in the dendritic areas in the NF-H positive cells and drastic decrease of Psd95 levels in the retina, as in the case of *OPA1* KO mice (59). Moreover, the *Prickle3* KO mice exhibited the abnormal vasculature, such as dilated and tortuous retinal vessels, with more branches, but no signs of fluorescein leakage in both eyes, consistent with pathological changes seen in the LHON patients (1,44,45). Finally, the *Prickle3* KO mice displayed the retina deficiencies, including the reductions in the scotopic b-wave of dark-adapted amplitude, photopic b-wave ERG amplitude for cone function, and maximal combined rod-cone responses of *Prickle3* KO mice eyes. These retinal deficiencies in the *Prickle3* KO mice were comparable with those in LHON patients and mouse mtDNA mutant model of LHON (3,4,18,56). In particular, biochemical and retinal deficiencies observed in the *Prickle3*$^{+/-}$ mice further confirmed the haploinsufficiency of *Prickle 3* mutation. Therefore, we concluded that the *Prickle3* knock-out mouse recapitulated the clinical phenotypes in LHON patients.

In summary, we identified an X-linked nuclear modifier gene *PRICKLE3* for the phenotypic manifestation of LHON-associated mtDNA mutations. The PRICKLE3 is directly linked to biogenesis of ATPase and mutated PRICKLE3 altered the assembly, stability and function of ATP synthase. The PRICKLE3 p.Arg53Trp is a haploinsufficient mutation which acted in synergy with m.11778G>A mutation and then deteriorated the mitochondrial dysfunctions necessary for the expression of LHON. The *Prickle3* knock-out mouse exhibited the pronounced decreases in the content of

fully assembled and functional ATP synthase, consistent with those in LHON patients. *Prickle3* knock-out mouse recaptured LHON phenotypes with the retina deficiencies. Our findings provide new insights into pathophysiology of LHON that were manifested by interactions between ND4 and X-linked PRICKLE3 mutations. Furthermore, the approach utilized in this study provides a paradigm for understanding the role of nuclear modifier gene in the pathogenic effects of mtDNA mutations and the mitochondrial functions in the RGCs.

**Methods**

*Families and subjects.* DNA samples used for this investigation were from 361 symptomatic and 234 asymptomatic members of 211 Han Chinese families, 58 symptomatic and 58 asymptomatic individuals from 58 Caucasian pedigrees carrying the m.11778G>A mutation and 1515 Han Chinese and 237 Caucasian control subjects lacking the m.11778G>A mutation (11,22,23,27,60). The ophthalmic examinations and other clinical evaluations of probands, other members of these families and control subjects were conducted as detailed elsewhere (23,27). Informed consent, blood samples, and clinical evaluations were obtained from all participants and families, under protocols approved by the Ethic Committees of Zhejiang University School of Medicine and Institutional Review Board of Cincinnati Children's Hospital Medical Center.

*Sequencing and genetic data analysis.* Whole exome sequencings of four members (III-14, III-15, II-7 and II-8) of SD1 pedigree were performed by BGI (Shenzhen, China). The data for these whole exome sequences were submitted into BioProject database (ID: PRJNA634625). High-quality genomic DNA (3 μg) was captured by hybridization using the SureSelect XT Human All Exon 50 Mb kit (Agilent Technologies, Santa Clara). Samples were prepared according to the manufacturer's instructions. Each captured library was run on a HiSeq 2000 instrument and sequences generated as 90 bp pair-end reads. An average of 82 million paired reads was generated per sample, the mean duplication rate was 13.45%, and 98.64% of targeted regions were covered by at least 70x mean depth. All sequencing reads were mapped to the human reference genome (GRCh37) at UCSC. Software SOAPsnp was used to assemble the consensus sequence and call genotypes in the target regions. GATK (IndelGenotyper V1.0) was used for indel detection. The threshold for filtering single-nucleotide

polymorphisms (SNPs) included the following criterion: SNP quality score should be ≥20; sequencing depth should be between 4 and 200; estimated copy numbers should be no more than 2 and the distance between two SNPs should be larger than 5. SNPs from these analyses were summarized in Supplemental Table 2. Variants were annotated by Annovar program. To further filter the SNP, the criteria for potential candidate variants were nonsynonymous or in splice sites within 6 bp of an exon, less than 1% mutant allele frequency in variant databases and co-segregated with the phenotype. The mutations were validated by Sanger sequencing in all family members and other unrelated samples.

Primers of *PRICKLE3* for Sanger sequencing was listed in Supplemental Table 3, including the primers for the genotyping of c.157C>T mutation in the exon 3. The entire mtDNA of 3 Chinese families carrying both PRICKLE3 c.157C>T and m.11778G>A mutations were analyzed as described elsewhere (29). The resulting sequences were compared with the updated consensus Cambridge sequence (GenBank accession number: NC_012920) (6). The copy numbers of mtDNA from mutant and control cell lines were determined as described elsewhere (61).

*Generation and genotyping of Prickle3 knockout mice.* All animal care protocols were approved by the Animal Care and Use Committee of Zhejiang University School of Medicine. C57BL/6J mice were originally purchased from Shanghai SLAC Laboratory Animal Co, Ltd (Shanghai). Sanger sequence analysis of *Crb1* gene failed to detect the Rd8 mutation in vendor lines of C57BL/6J mice (62). *Prickle3* knock-out mice were generated using CRISPR-Cas9 approach. The targeting gRNA and donor oligo for *Prickle3* were listed in Supplemental Table 3. Cas9 mRNA, gRNAs and donor vector were mixed at different concentrations and co-injected into the cytoplasm of fertilized eggs at the one-cell stage. After injection, surviving zygotes were transferred

into the oviducts of pseudopregnant females. The genotypes for the *Prickle3*$^{+/-}$, *Prickle3*$^{-/-}$ *and Prickle3*$^{-/o}$ were confirmed by PCR amplification and direct sequencing. Mouse bearing the *Prickle3* 13bp deletion was selected and then mated with C57BL/6J female mice.

*Cell lines and culture conditions.* Lymphoblastoid cell lines were generated from members of SD1 pedigree [two affected individuals (II-8 and III-2) carrying both m.11778G>A and heterozygous c.157C>T mutations, two affected members (III-13 and III-14) carrying both m.11778G>A and hemizygous c.157C>T mutations, two vision normal subjects (II-9,III-15) carrying only m.11778G>A mutation, one individual (IV-3) carrying only heterozygous c.157C>T mutation] and two genetically unrelated control subjects (C1-2 and WZ209) lacking both mutations, as detailed previously (63). Lymphoblastoid cell lines were grown in RPMI 1640 medium (Invitrogen, Waltham), supplemented with 10% fetal bovine serum (FBS). HeLa and 293T cell lines were grown in DMEM (Corning Inc, Corning), supplemented with 10% FBS.

*Western blot and immunoprecipitation assays*. Western blot analysis was performed using 20 μg of total cellular proteins isolated from human cell lines or mice tissues, as detailed elsewhere (15,64). The antibodies used for this investigation were summarized in Supplemental Table 5. Peroxidase Affini Pure goat anti-mouse IgG and goat anti-rabbit IgG (Jackson ImmunoResearch Laboratories, West Grove) were used as a secondary antibody and protein signals were detected using the ECL system (CWBIO, Beijing). Quantification of density in each band was as detailed previously (15,64).

For the immunoprecipitation (IP) analysis, mitochondria were extracted from 293T cell line after transfected with PRICKLE3-HA for 36 hours as described

elsewhere (65). Five μg mitochondrial proteins were solubilized in 1ml PBS containing 0.5% dodecyl-D-maltoside on ice for 30 min and centrifuged at 20,000 g for 10 min at 4°C. The supernatants were incubated with 10 μl of beads (cross-linked to 25 μg of monoclonal antibody, anti-HA or anti-ATPase complex) for overnight at 4°C with rotation. Beads were washed for four times, and then boiled for 5 min after SDS loading added. Finally, the IP fractions were analyzed by Western blot analysis.

*Enzymatic activity Assays.* The enzymatic activities of OXPHOS complexes I, II, III, IV and V were measured as detailed elsewhere (66,67). For evaluating the activity of complex V in gel, 20 μg total cellular protein samples from human cell lines or mice tissues were loaded, and run at 150 V in light blue cathode buffer for 1h, then at 250 V in clear cathode buffer. The native gels were prewashed in cold water, and then incubated with the substrates of complex V in the buffer containing 35 mM Tris, 270 mM glycine, 14 mM $MgSO_4$, 10 mM ATP, 0.2% $Pb(NO_3)_2$ at room temperature overnight. The gel was washed with 50% methanol for 3 times. Images were captured and quantified as described elsewhere (37).

*Measurements of oxygen consumption.* The rates of oxygen consumption (OCR) in mutant and control cell lines were measured with a Seahorse Bioscience XF-96 extracellular flux analyzer (Seahorse Bioscience), as detailed elsewhere (68-70).

*ATP measurements.* The CellTiter-Glo® Luminescent Cell Viability Assay kit (Promega) was used for the measurement of cellular and mitochondrial ATP levels, according to the modified manufacturer's instructions (65,68).

*Stability analysis of ATPase by Native PAGE.* The stability of assembled ATPase was analyzed by mitochondria isolated from human cell lines and mice liver using blue native gel electrophoresis (31,32). In brief, 400 μg mitochondria were solubilized in 0.5% DDM solution containing 50 Mm NaCl, 50 mM imidazole, 2 mM 6-

aninohexanoic acid and 1 mM EDTA (pH7.4) on ice for 20 min. After removing insoluble material by centrifugation, 10 μg of lysed mitochondria from each sample were loaded to 3-12% gradient Native PAGE Bis-Tris gel, and run at 150 V in dark blue cathode buffer for 1 h and then 250 V in light blue running buffer for 1.5 h at 4°C. The native gels were then prewashed in a transfer buffer (25 mM Tris, 192 mM glycine, 20% methanol), and transferred to the polyvinylidene fluoride membrane at 30V overnight for immunoblotting.

*ATP measurements.* The CellTiter-Glo® Luminescent Cell Viability Assay kit (Promega) was used for the measurement of cellular and mitochondrial ATP levels, according to the modified manufacturer's instructions (64,68).

*Immunofluorescence and Immunohistochemistry.* For NF-H flat-mount staining, whole mice retina (at 8 weeks) were fixed in 4% paraformaldehyde at 4°C for 2 h, permeabilized with 0.2% Tween for 1 hour, blocked with 5% FBS serum buffer (+0.2% Triton X-100 in PBS) at room temperature for 1 hour, and followed by incubating with mouse anti-NF-H (1:1000, Cell Signaling Technology) at 4°C overnight and then secondary antibody, Alexa Fluor 488 goat anti-mouse IgG, for 2 h. Retinas were washed again three times for 3 h, and mounted in a mounting medium. Images were taken by Leica DM4000B-M. Nikon NIS-elements imaging software was used to automatically measure cell body area and dendritic field in the RGCs as described previously (41,71).

Cross-sections of retina staining with Brn3a and tubulin were performed as detailed previously (38, 39). Eye cups were dissected and immersed in 4% paraformaldehyde in PBS for 24 h, and then embedded in O.C.T. compound (Thermo fisher, Watham) after infiltrating with 30% sucrose overnight. Transverse sections of the retina (10 μm thick) were mounted onto slides and blocked with 20% fetal calf serum in PBS for 1 h. Primary

antibodies, anti-Brn3a (1:500) and anti-*β*-III-tubulin (1:2500 (Abcam, Cambridge, MA), were incubated with at 4°C overnight, and then the secondary antibodies, Alexa Fluor 488 goat anti-mouse IgG and Alexa Fluor 594 goat anti-rabbit IgG. Imaged were taken by Leica DM4000B-M (Leica Camera, Wetzlar) and Olympus Fluoview FV1000 (Olympus Corporation, Tokyo) microscopes with DAPI for nuclei.

*Fluorescein Angiography.* Fluorescent angiography of eyes was carried out in *Prickle3* KO and WT mice (at 8 weeks) using the Micron III camera (Phoenix Research Laboratories, Inc., Pleasanton) as described previously (72). Pupils were dilated with 1% tropicamide (Bausch & Lomb, Tampa) followed by application of GenTeal Lubricant Eye Gel (Alcon, Ft. Worth). Systane lubricant eye drops (Alcon) were applied to keep the cornea moist. Mouse pupils were then intraperitoneally injected with 25% Angiofluor TM (Alliance Pharmaceutical, Inc., San Diego) at a dose of 0.01 ml per 5 μg of mouse body weight. Photos were taken with a camera containing a barrier filter for fluorescein angiography.

*Retinal vessel labeling.* Whole mice retina were fixed for half hour and blocked with 5% FBS serum buffer at 4°C overnight, then equilibrated with the solution (1 μM $MgCl_2$, 1μM $CaCl_2$, 0.1 μM $MnCl_2$, 0.1% Tritron X-100 in PBS) 1h at room temperature. After incubating with FITC-conjugated isolectin B4 (1:50 in blocking buffer (Sigma-Aldrich, St. Louis) at 4°C for overnight, the retinas were washed, mounted, and then imaged by Leica DM4000B-M.

*ERGs measurement.* ERGs of mice (at 8 weeks) were recorded as previously described (41). Both the scotopic and photopic ERGs were recorded with a well-established Ganzfeld Q450 dome stimulating and recording system. Mice were dark-adapted, anesthetized with Ag/AgCl wire loop electrode placed over the cornea.

*Statistics.* Statistical analysis was performed using the unpaired, two-tailed

Student's *t*-test contained in the Microsoft-Excel program (version 2017). Differences were considered significant at a $P<0.05$.

*Study approval.* Informed consent in writing prior to their participation in this study were obtained from members of families and control subjects, under protocols approved by the Ethic Committees of Zhejiang University School of Medicine and Institutional Review Board of Cincinnati Children's Hospital Medical Center. Furthermore, all experiments involving mice were approved by the Institutional Animal Care and Use Committee, Zhejiang University School of Medicine.

**Author contributions**

M.X.G. and P.J. designed the experiments, monitored the project progression, data analysis and interpretation. J.Y., J.L., C.A. performed the biochemical analyses, J.Y., Y, J., J.L., L.Z., X.J., and X.Z. performed the whole exome sequence and mutational screening; X.L, J.Y., C.A., Z.N., C.W. and S.M. carried out the mouse experiments; Y.J., J.Z., F.Z., X.Z., M.Z. and T.H. carried out the clinical evaluation and recruited LHON patients; J.Y. and M.W. performed the data analysis. P.J. prepared the initial draft of the manuscript. M.X.G. made the final version of the manuscript. All authors reviewed the manuscript.

**Acknowledgments**

We are grateful to patients and their family members for their participation. This work was supported by National Key Research and Development Program of China grant 2018YFC1004802 to M.X.G., grants 31671303, 31970557, 81900904 from the Natural Science Foundation of China to P.J., M.X.G. and J.Y., respectively, and the National Key Technologies R&D Program of China grant 2012BAI09B03 M.X.G. and P.J., and the Zhejiang Provincial Program for the Cultivation of High-level Innovative Health talents to P.J.

## REFERENCE


1. Wallace DC, Lott MT. Leber Hereditary Optic Neuropathy: Exemplar of an mtDNA Disease. *Handb Exp Pharmacol.* 2017; 240: 339-376.

2. Howell N. Leber hereditary optic neuropathy: respiratory chain dysfunction and degeneration of the optic nerve. *Vision Res*. 1998; 38(10):1495-1504.

3. Sadun AA, La Morgia C, Carelli V. Leber's Hereditary Optic Neuropathy. *Curr Treat Options Neurol.* 2011; 1391(1): 109-117.

4. Newman NJ. Hereditary optic neuropathies: from the mitochondria to the optic nerve. *Am J Ophthalmol.* 2005; 1409(3):517-523.

5. Carelli V, La Morga C, Valentino ML, Barboni P, Ross-Cisneros FN, Sadun AA. Retinal ganglion cell neurodegeneration in mitochondrial inherited disorders. *Biochim Biophys Acta.* 2009; 1787(5):518-528.

6. Andrews RM, Kubacka I, Chinnery PF, Lightowlers RN, Turnbull DM, Howell N. Reanalysis and revision of the Cambridge reference sequence for human mitochondrial DNA. *Nat Genet.* 1999; 239(1): 147.

7. Wallace DC, et al. Mitochondrial DNA mutation associated with Leber's hereditary optic neuropathy. *Science.* 1988; 24(4884): 1427-1430.

8. Ruiz-Pesini E, et al. An enhanced mitomap with a global mtDNA mutational phylogeny. *Nucleic Acids Res.*2007; 35: D823-D828.

9. Brown MD, Torroni A, Reckord CL, Wallace DC. Phylogenetic analysis of Leber's hereditary optic neuropathy mitochondrial DNA's indicates multiple independent occurrences of the common mutations. *Hum Mutat.* 1995(4); 6:311-325.

10. Yu-Wai-Man P, Griffiths PG, Hudson G, Chinnery PF. Inherited mitochondrial optic neuropathies. *J Med Genet.* 2009; 46(3): 145-158.

11. Jiang P, et al. Prevalence of mitochondrial ND4 mutations in 1281 Han Chinese subjects with Leber's Hereditary Optic Neuropathy. *Invest Ophthalmol Vis Sci.* 2015(8); 56: 4778-4788.

12. MashimaY, et al. Spectrum of pathogenic mitochondrial DNA mutations and clinical features in Japanese families with Leber's hereditary optic neuropathy. *Curr Eye Res.* 1998; 17(4): 403-408.

13. Brown MD, Trounce IA, Jun AS, Allen JC, Wallace DC. Functional analysis of lymphoblast and cybrid mitochondria containing the 3460, 11778, or 14484 Leber's hereditary optic neuropathy mitochondrial DNA mutation. *J Biol Chem.* 2000; 275(51): 39831-39836.

14. Hofhaus G, Johns DR, Hurkoi O, Attardi G, Chomyn A. Respiration and growth defects in transmitochondrial cell lines carrying the 11778 mutation associated with Leber's hereditary optic neuropathy. *J Biol Chem.* 1996; 271(22): 13155-13161.

15. Jiang P, et al. The exome sequencing identified the mutation in YARS2 encoding the mitochondrial tyrosyl-tRNA synthetase as a nuclear modifier for the phenotypic manifestation of Leber's hereditary optic neuropathy-associated mitochondrial DNA mutation. *Hum Mol Genet.* 2016(3); 25:584-596.

16. Qian Y, Zhou X, Liang M, Qu J, Guan MX. The altered activity of complex III may contribute to the high penetrance of Leber's hereditary optic neuropathy in a Chinese family carrying the ND4 G11778A mutation. *Mitochondrion.* 2011; 11(6): 871-877.

17. Newman NJ, Lott MT, Wallace DC. The clinical characteristics of pedigrees of Leber's hereditary optic neuropathy with the 11778 mutation. *Am J Ophthalmol.* 1991; 111(6):750-762.

18. Riordan-Eva P, Sanders MD, Govan GG, Sweeney MG, Dacosta J, Harding AE. The clinical features of Leber's hereditary optic neuropathy defined by the presence of a pathogenic mitochondrial DNA mutation. *Brain.* 1995;118(Pt 2): 319-337.

19. Bu XD, Rotter JI. X chromosome-linked and mitochondrial gene control of Leber hereditary optic neuropathy: evidence from segregation analysis for dependence on X chromosome inactivation. *Proc Natl Acad Sci USA.* 1991; 88(18): 8198-8202.

20. Hudson G, et al. Identification of an X-chromosomal locus and haplotype modulating the phenotype of a mitochondrial DNA disorder. *Am J Hum Genet.* 2005; 77(6): 1086–1091.

21. Shankar SP, et al. Evidence for a novel X-linked modifier locus for Leber hereditary optic neuropathy. *Ophthalmic Genet.* 2008; 29(1): 17-24.

22. Ji Y, et al. Mitochondrial ND1 variants in 1281 Chinese subjects with Leber's hereditary optic neuropathy. *Invest Ophthalmol Vis Sci.* 2016; 56(6)*:* 2377-2389.

23. Liang M, et al. Frequency and spectrum of mitochondrial ND6 mutations in 1218 Han Chinese subjects with Leber's hereditary optic neuropathy. *Invest Ophthalmol Vis Sci.* 2014; 55(3):1321-1331.

24. Collu GM, et al. Prickle is phosphorylated by Nemo and targeted for degradation to maintain Prickle/Spiny-legs isoform balance during planar cell polarity establishment. *PLoS Genet*. 2018; 14(5): e1007391.

25. Ehaideb SN, et al. Prickle modulates microtubule polarity and axonal transport to ameliorate seizures in flies. *Proc Natl Acad Sci USA.* 2014; 111(30): 11187-11192.

26. Ossipova O, Chu, CW, Fillatre J, Brott BK, Itoh K, Sokol SY. The involvement of PCP proteins in radial cell intercalations during *Xenopus* embryonic development. *Dev Biol.* 2015; 408(2): 316-327.

27. Zhou X, et al. Very high penetrance and occurrence of Leber's hereditary optic neuropathy in a large Han Chinese pedigree carrying the ND4 G11778A mutation. *Mol Genet Metab.* 2010; 100(4): 379-384.

28. Tao H, et al. Mutations in prickle orthologs cause seizures in flies, mice, and humans. *Am J Hum Genet.* 2011; 88(2): 138-149.

29. Rieder MJ, Taylor SL, Tobe VO, Nickerson DA. Automating the identification of DNA variations using quality-based fluorescence re-sequencing: analysis of the human mitochondrial genome. *Nucleic Acids Res.* 1998; 26(4):967-973.

30. Claros MG, Vincens P. Computational method to predict mitochondrially imported proteins and their targeting sequences. *Eur J Biochem.* 1996; 241(3):779-786.

31. Jha P, Wang X, Auwerx J. Analysis of mitochondrial respiratory chain supercomplexes using blue native polyacrylamide gel electrophoresis (BNPAGE). *Curr Protoc Mouse Biol.* 2016; 6(1): 1-14.

32. Wittig I, Braun HP, Schägger H. Blue native PAGE. *Nat Protoc.* 2006; 1(1): 418-428.

33. Jonckheere AI, Smeitink JA, Rodenburg RJ. Mitochondrial ATP synthase: architecture, function and pathology. *J Inherit Metab Dis.* 2012; 35(2): 211-225.

34. Junge W, Nelson N. ATP synthase. *Annu Rev Biochem.* 2015; 84: 631–657.

35. Naumenko N, Morgenstern M, Rucktäschel R, Warscheid B, Rehling P. INA complex liaises the $F_1F_0$-ATP synthase membrane motor modules. *Nat Commun.* 2017; 8(1): 1237.

36. Guo H, Bueler SA, Rubinstein JL. Atomic model for the dimeric $F_0$ region of mitochondrial ATP synthase. *Science.* 2017; 358(6365): 936-940.

37. He J, et al. Assembly of the membrane domain of ATP synthase in human mitochondria. *Proc Natl Acad Sci USA.* 2018; 115(12): 2988-2993.

38. McCulloch DL, et al. ISCEV Standard for full-field clinical electroretinography (2015 update). *Doc Ophthalmol.* 2015; 130(1):1-12.

39. Badea TC, Cahill H, Ecker J, Hattar S, Nathans J. Distinct roles of transcription factors brn3a and brn3b in controlling the development, morphology, and function of retinal ganglion cells. *Neuron.* 2009; 61(6): 852-64.

40. Goel M, Dhingra NK. Müller glia express rhodopsin in a mouse model of inherited retinal degeneration. *Neuroscience.* 2012; 225:152-161.

41. Song, L, Yu A, Murray K, Cortopassi G. Bipolar cell reduction precedes retinal ganglion neuron loss in a complex 1 knockout mouse model. *Brain Res.* 2017; 1657: 232-244.

42. Li, X., et al. Gene therapy rescues cone structure and function in the 3-month-old rd12 mouse: a model for midcourse RPE65 leber congenital amaurosis. *Invest ophthalmol Vis Sci.* 2011; 52(1): 7-15.

43. Zuercher J, Fritzsche M, Feil S, Mohn L, Berger W. Norrin stimulates cell proliferation in the superficial retinal vascular plexus and is pivotal for the recruitment of mural cells. *Hum Mol Genet.* 2012; 21(12): 2619-2630.

44. Carelli V, La Morgia C, Ross-Cisneros FN, Sadun AA. Optic neuropathies: the tip of the neuro degeneration iceberg. *Hum Mol Genet.* 2017; 26(R2): R139-R150.

45. Kerrison JB, Newman NJ. Clinical spectrum of Leber's hereditary optic neuropathy. *Clin Neurosci*. 1997; 4(5): 295-301.

46. Harding AE, Sweeney MG, Govan GG, Riordan-Eva P. Pedigree analysis in Leber hereditary optic neuropathy families with a pathogenic mtDNA mutation. *Am J Hum Genet*. 1995; 57(1):77–86.

47. Rak M, Gokova S, Tzagoloff A. Modular assembly of yeast mitochondrial ATP synthase. *EMBO J.* 2011; 30(5): 920-930.

48. Vrbacký M, et al. Knockout of Tmem70 alters biogenesis of ATP synthase and leads to embryonal lethality in mice. *Hum Mol Genet.* 2016; 25(21): 4674-4685.

49. Wang ZG, White PS, Ackerman SH. Atp11p and Atp12p are assembly factors for the F(1)-ATPase in human mitochondria. *J Biol Chem.* 2001; 276(33): 30773-30778.

50. De Meirleir L, et al. Respiratory chain complex V deficiency due to a mutation in the assembly gene ATP12. *J Med Genet.* 2004; 41(2):120-124

51. Spiegel R, et al. *TMEM70* mutations are a common cause of nuclear encoded ATP synthase assembly defect: further delineation of a new syndrome. *J Med Genet.* 2011; 48(3): 177-182.

52. Houstek J, et al. A novel deficiency of mitochondrial ATPase of nuclear origin. *Hum Mol Genet.* 1999; 8(11):1967-1994.

53. Trounce I, Neill S, Wallace DC. Cytoplasmic transfer of the mtDNA nt 8993 T>G (ATP6) point mutation associated with Leigh syndrome into mtDNA-less cells demonstrates cosegregation with a decrease in state III respiration and ADP/O ratio. *Proc Natl Acad Sci USA*. 1994; 91(18): 8334-8338.

54. Bartha I, di Iulio J, Venter JC, Telenti A. Human gene essentiality. *Nat Rev Genet*. 2018;19(1):51-62.

55. Jonckheere AI, et al. Restoration of complex V deficiency caused by a novel deletion in the human TMEM70 gene normalizes mitochondrial morphology. *Mitochondrion.* 2011; 11(6): 954-963.

56. Lin CS, et al. Mouse mtDNA mutant model of Leber hereditary optic neuropathy. *Proc Natl Acad Sci USA.* 2012; 109(49): 20065-20070.

57. Yu AK, et al. Mitochondrial complex I deficiency leads to inflammation and retinal ganglion cell death in the Ndufs4 mouse. *Hum Mol Genet*. 2015; 24(10):2848-2860.

58. Chu CW, Sokol SY. Wnt proteins can direct planar cell polarity in vertebrate ectoderm. *Elife.* 2016; 5: e16463.

59. Williams PA, Morgan JE, Votruba M. Opa1 deficiency in a mouse model of dominant optic atrophy leads to retinal ganglion cell dendropathy. *Brain.* 2010; 133(10): 2942-2951.

60. Ji Y, et al. Contribution of mitochondrial ND1 3394T>C mutation to the phenotypic manifestation of Leber's hereditary optic neuropathy. *Hum Mol Genet.* 2019; 28(9):1515-1529.

61. Zhang J, et al. A novel ADOA-associated OPA1 mutation alters the mitochondrial function, membrane potential, ROS production and apoptosis. *Sci Rep.* 2017; 7(1):5704.

62. Mattapallil MJ, et al. The Rd8 mutation of the Crb1 gene is present in vendor lines of C57BL/6N mice and embryonic stem cells, and confounds ocular induced mutant phenotypes. *Invest Ophthalmol Vis Sci*. 2012;53(6):2921-2027.

63. Miller G, Lipman M. (1973) Release of infectious Epstein–Barr virus by transformed marmoset leukocytes. *Proc Natl Acad Sci USA*. 1973; 709(1): 190–194.

64. Zhou M, et al. (2018) A hypertension-associated mitochondrial DNA mutation introduces an $m^1G37$ modification into $tRNA^{Met}$, altering its structure and function. *J Biol Chem*. 2018; 293(4): 1425-1438.

65. Ausenda C, Chomyn A. Purification of mitochondrial DNA from human cell cultures and placenta. *Methods Enzymol.* 1996; 264: 122-128.

66. Birch-Machin MA, Turnbull DM. Assaying mitochondrial respiratory complex activity in mitochondria isolated from human cells and tissues. *Methods Cell Biol.* 2001; 65: 97-117.

67. Zhang J, et al. Leber's hereditary optic neuropathy (LHON)-associated ND5 12338T > C mutation altered the assembly and function of complex I, apoptosis and mitophagy. *Hum Mol Genet*. 2018; 27(11):1999-2011.

68. Gong S, et al. (2014) A deafness-associated $tRNA^{His}$ mutation alters the mitochondrial function, ROS production and membrane potential. *Nucleic Acids Res.* 2014; 42(12): 8039-8048.

69. Dranka BP, et al. Assessing bioenergetic function in response to oxidative stress by metabolic profiling. *Free Radic Biol Med.* 2011; 51(9): 1621-1635.

70. Jiang P, et al. Biochemical evidence for a mitochondrial genetic modifier in the phenotypic manifestation of Leber's hereditary optic neuropathy-associated mitochondrial DNA mutation. *Hum Mol Genet. 2016;* 25(16): 3613-3625.

71. Leung CK, et al. Long-term *in vivo* imaging and measurement of dendritic shrinkage of retinal ganglion cells. *Invest Ophthalmol Vis Sci.* 2011;52(3):1539-1547

72. Spaide PF, Klancnik JM Jr., Cooney MJ. Retinal vascular layers imaged by fluorescein

angiography and optical coherence tomography angiography. *JAMA Ophthalmol*. 2015; 133(1): 45-50.

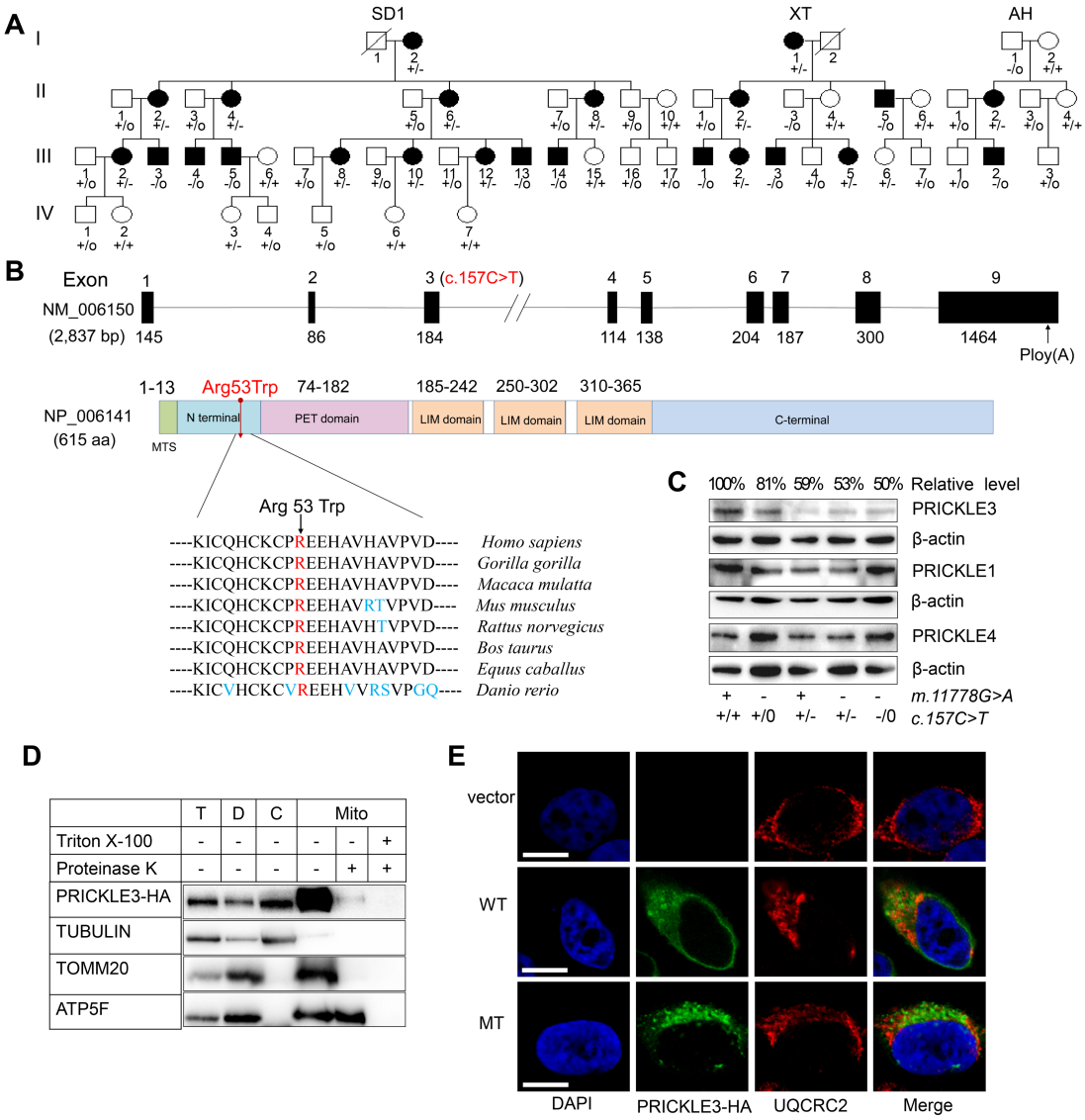


**Figure 1. Identification of PRICKLE3 Arg53Trp mutation. (A)** Three Chinese pedigrees with LHON. Vision-impaired individuals were indicated by blackened symbols. Individuals harboring hemizygous (-/0), heterozygous (+/-) *PRICKLE3* (c.157C>T, p.Arg53Trp) mutation and wild-type (+/+ or +/0) were indicated. **(B)** Scheme for the structure of *PRICKLE3* and its product, multiple sequence alignment of homologs. **(C)** Western blot analysis of PRICKLE3, PRICKLE1 and PRICKLE4 in various lymphoblastoid cell lines. The levels of these proteins were quantified in the linear range of the sample loading and expressed as percentages of the average values for the control cell lines. **(D)** Subcellular localization of PRICKLE3 by Western blotting with anti-HA, TOM22 (outer mitochondrial membrane), ATP5F (inner mitochondrial membrane) and Tubulin (cytosol). D, debris; C, cytosol; Mito, mitochondria; T, total cell lysate. Isolated mitochondria were treated with (+) or without (-) 1% Triton X-100 (Tx) followed by Proteinase K digestion, respectively. **(E).** Subcellular localization of PRICKLE3 by immunofluorescence in HeLa cells. HA-PRICKLE3 WT or MT (green), UQCRC2 (red), and DAPI (blue). Scale bar: 10 μm.

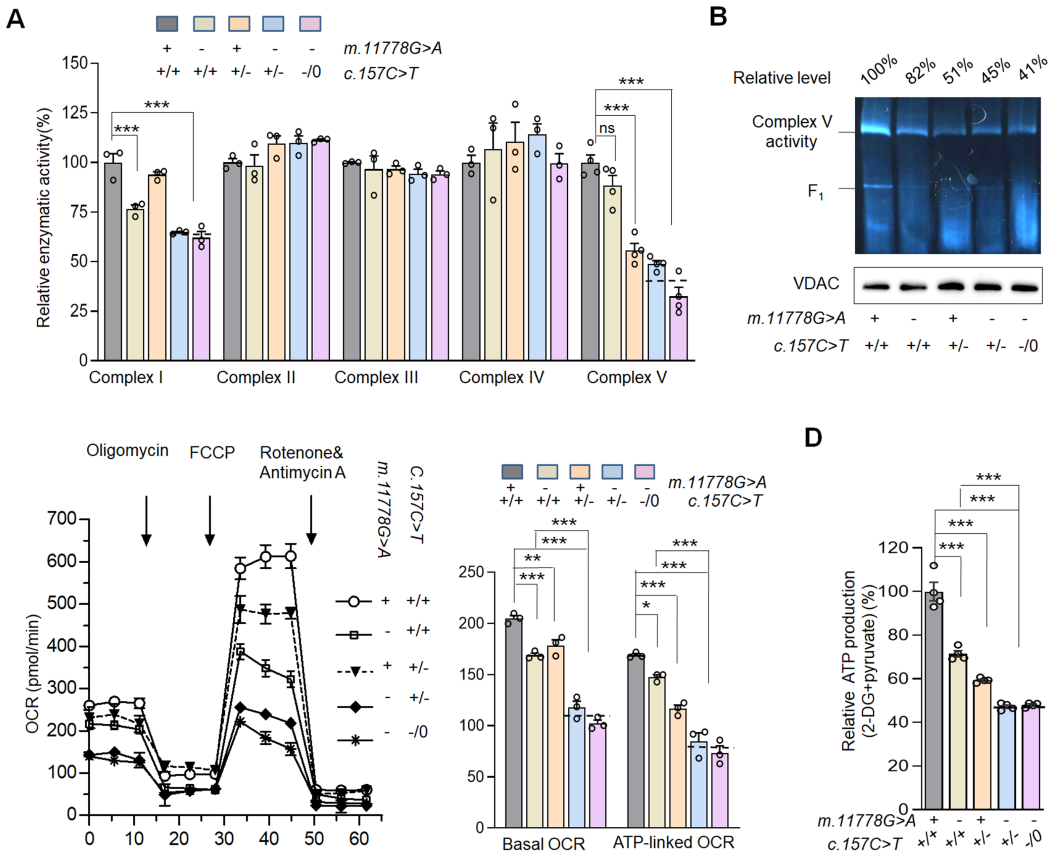


**Figure 2. The p.Arg53Trp mutation caused the defective activity of mitochondrial ATPase. (A)** Enzymatic activities of respiratory chain complexes in mitochondria isolated from various cell lines. Data are mean ± standard error of mean (SEM) of triplicate for complex I to IV and of quadruplicate for complex V. **(B)** In-gel activity of ATPase. **(C)** The rates of OCR ($O_2$ consumption) in the various cell lines using different inhibitors. Basal OCR was determined as OCR before oligomycin minus OCR after rotenone/antimycin A. ATP-lined OCR was determined as OCR before oligomycin minus OCR after oligomycin. Data are mean ± SEM of triplicates. **(D)** Measurement of mitochondrial ATP levels using a bioluminescence assay. Cells were incubated with 5 mM 2-deoxy-d-glucose plus 5 mM pyruvate to determine ATP generation under mitochondrial ATP synthesis. Average rates of ATP level per cell line and are shown. Data are mean ± SEM of triplicates. Dashed lines indicated the mean values of enzymatic activities or OCRs in *PRICKLE3*$^{+/-}$ and *PRICKLE3*$^{-/0}$ cell lines. *P* indicates the significance, according to the *t*-test, of the differences between mutant and control cell lines. **P*<0.05, ***P*<0.01, *** *P*<0.001, ns, no statistically significant.

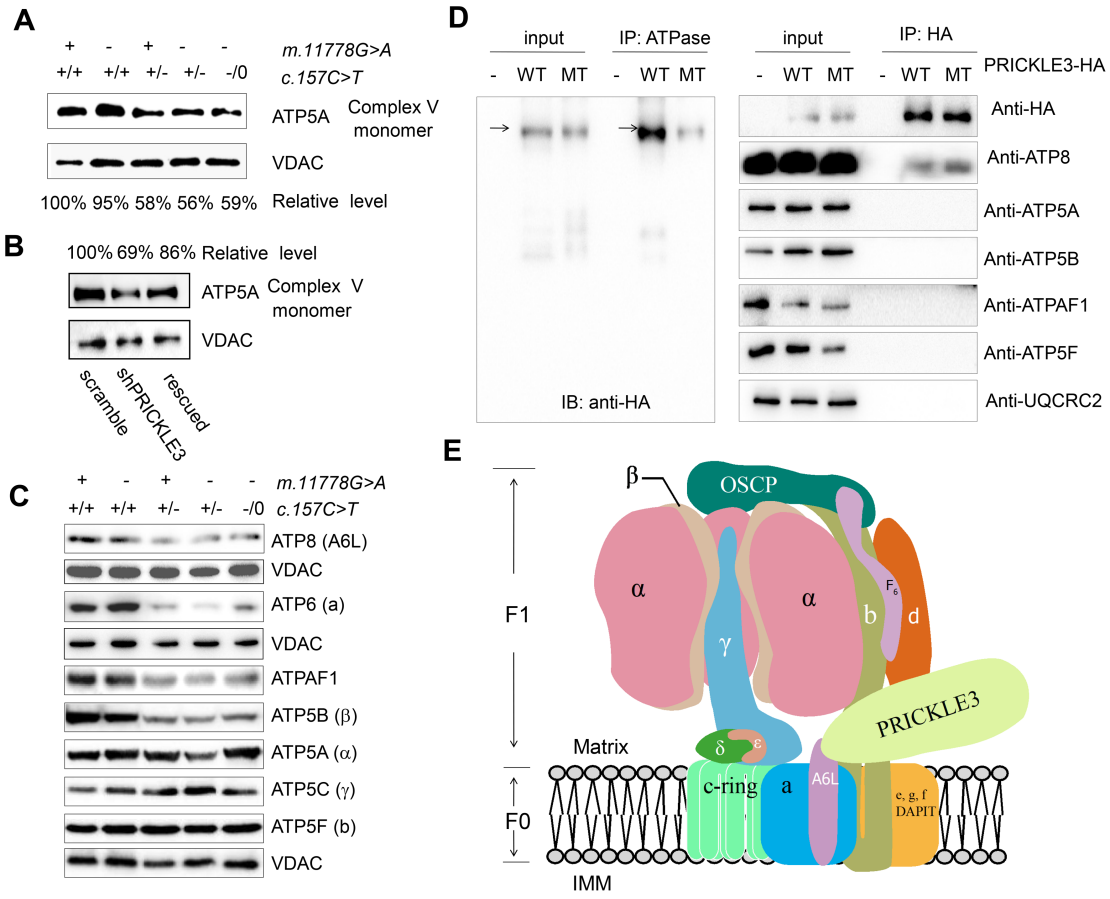


**Figure 3. The p.Arg53Trp mutation altered the assembly and stability of ATP synthase.** **(A,B)** The stability of fully assembly of ATP synthase monomer. Mitochondria isolated from various lymphoblastoids cell lines **(A)** and Hela cells, which were transfected by shRNA (PRICKLE3 and Scramble) and rescued by WT-PRICKLE3 **(B)**, subjected to BN-PAGE and hybridized with anti-ATP5A antibody and VDAC as internal control. Data are mean ±SEM of triplicates. **(C)** Immunoblot analysis of subunits of ATP synthase. Total cellular proteins in various lymphoblastoid cell lines were electrophoresed with PAGE and hybridized with ATP6, ATP8, ATPAF1, ATP5B, ATP5A, ATP5C, ATP5F antibodies and VDAC as a loading control, respectively. **(D)** Physical interaction of PRICKLE3 with ATP8 (A6L). Isolate mitochondria from HEK293T cells, transiently expressing with wild type (WT), mutant (MT) PRICKLE3-HA and empty vector, were solubilized with 0.5% DDM. Lysate proteins and immuno-precipitated with ATP synthase immunocapture kit (left), HA-antibody (right), respectively. Antibodies: anti-HA, anti-ATP8, ATP5A, ATP5B, ATP5F, ATPAF1 for complex V and anti-UQCRC2 for complex III were used respectively. **(E)** Proposed model for the direct interaction between PRICKLE3 and ATPase ($F_0$: a, b, 8/A6L, d, e, f, g, DAPIT; $F_1$:α, β, γ, δ, ε). Matrix, mitochondrial matrix; IMM, inner mitochondrial membranes. $F_0F_1$-ATP structural model was modified from He, *et al* (2018) (37).

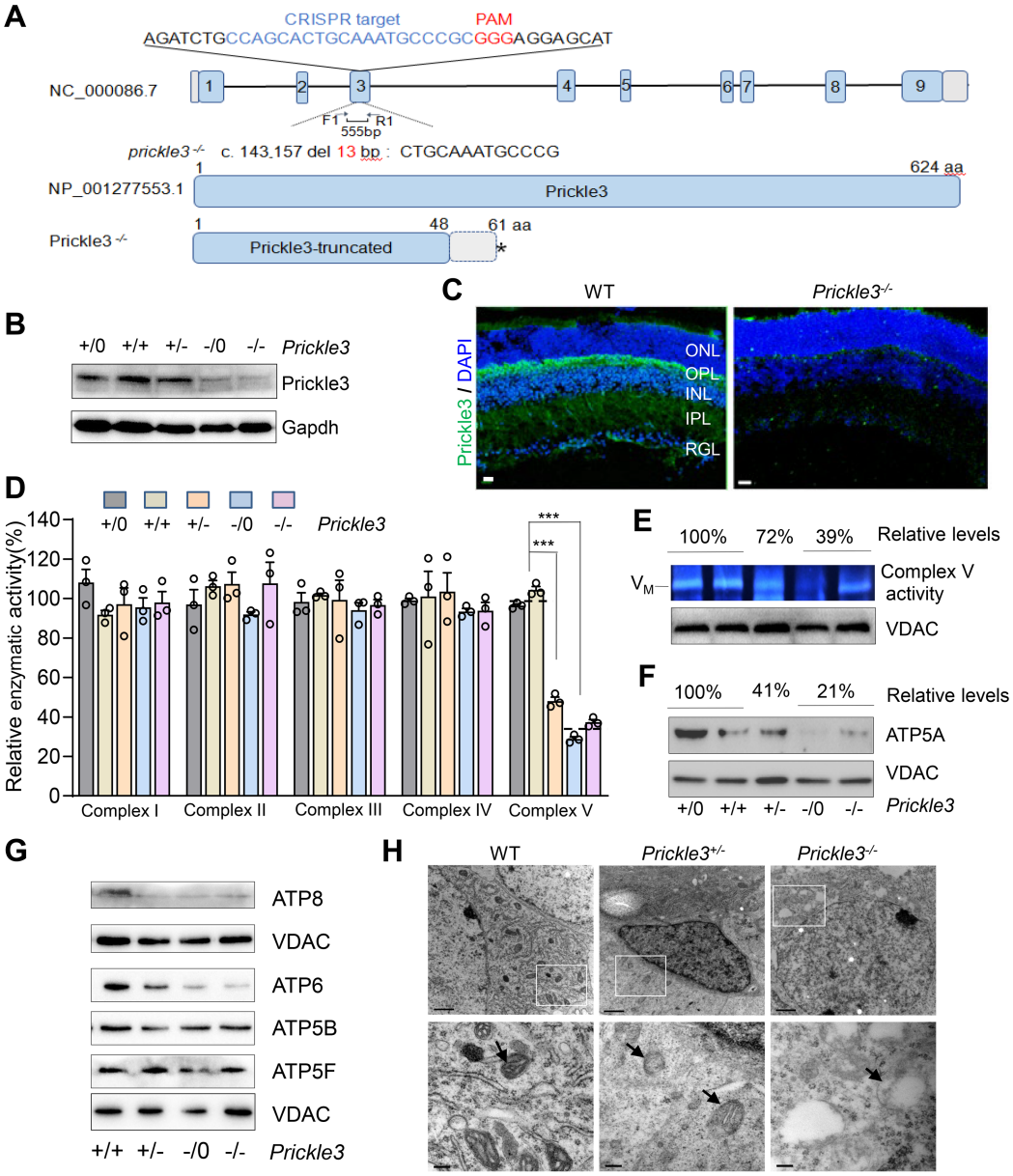


**Figure 4. The altered activity and assembly of complex V in retina from *Prickle3* knock-out mice. (A)** Schema of generation of *Prickle3* knock-out mice (C57BL/6J) using CRISPR/Cas9 system. A 13 bp deletion was produced in the exon 3 (c.144_158 nt) of *Prickle3*, resulting in a truncating protein with 60 amino acids. **(B)** Levels of Prickle3 in retinas from different genotype of mice with 8 weeks. **(C)** Prickle3 expression in retina of WT and *Prickle3*$^{-/-}$ mice by immunolabeling analysis. ONL, outer nuclear layer; OPL, outer plexiform layer; INL, inner nuclear layer; IPL, inner plexiform layer; RGL, ganglion cell layer. Scale bar: 10 μm. **(D)** Enzymatic activities of complexes I, II, III, IV and V in mitochondria isolated from the livers of *Prickle3* KO and WT mice. Data are mean ±SEM of triplicates. Dashed lines indicated the mean values of enzymatic activities in samples of *Prickle3*$^{-/0}$ and *Prickle3*$^{-/-}$ mice.*$P$<0.05, **$P$<0.01, ***$P$<0.001. **(E)** In-gel activity of ATPase in the livers of *Prickle3* KO and WT mice. **(F)** Assembly of ATP synthase monomer using BN-PAGE analysis in the liver mitochondria of *Prickle3* KO and WT mice. **(G)** Levels of ATP8, ATP6, ATP5A and ATP5F in the retinas of *Prickle3* KO and WT mice. **(H)** Mitochondrial morphology in RGCs by transparence electron microscopy. Arrows indicated mitochondria. Scale bar: 1 μm (upper panel), 0.2μm (lower panel).

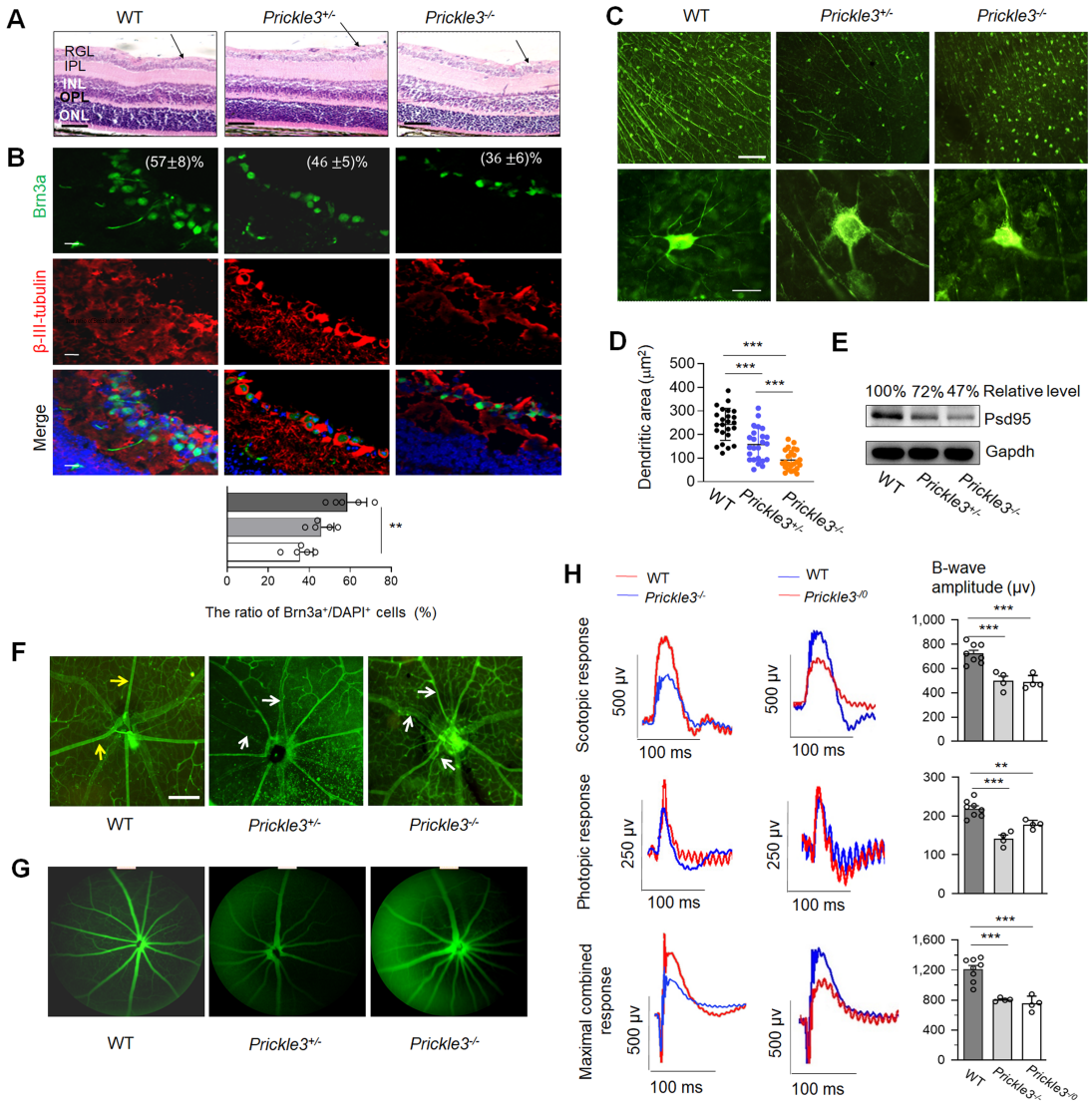


**Figure 5. Retinal deficiencies in *Prickle3* knockout mice at postnatal 8 weeks. (A)** Retina sections staining with Hematoxylin and eosin (HE) in WT, *Prickle3*$^{+/-}$ and *Prickle3*$^{-/-}$ mice. Arrows indicate RGC layer. Bar: 100 μm. **(B)** RGC cells staining with Brn3a (green) with *β*-III-tubulin (red) and DAPI (blue). The ratios of Brn3a$^{+}$/DAPI$^{+}$ cells in the RGC layer of WT (n=10), *Prickle3*$^{+/-}$ (n=10) and *Prickle3*$^{-/-}$ (n=10) mice were (57±8)%, (46±5)% and (36±6)% from 5 cross sections of 10 eyes for each genotypic mice sample (lower panel), respectively. Bar: 20 μm. (C) Neurofilaments staining of the whole mount retina with anti-NF-H antibody, and the neurons (NF positive) with their dendrites in higher magnification. Bar: 200 μm (upper panel); 50 μm (lower panel). **(D)** The mean dendritic areas measured from 24 NF-H positive cells in WT (n=24), *Prickle3*$^{+/-}$ (n=24) and *Prickle3*$^{-/-}$ mice (n=24). Data are mean± SEM. **(E)** Expression of postsynaptic density-95 (Psd95) in WT, *Prickle*$^{+/-}$ and *Prickle3*$^{-/-}$ retinas. **(F)** Retinal vasculatures labeling with Isolectin B4. White arrows indicated tortuous vessels in *Prickle3*$^{+/-}$ and *Prickle3*$^{-/-}$ mice. Bar: 200 μm. **(G)** Fluorescent angiography of eyes in the WT, *Prickle3*$^{+/-}$ and *Prickle3*$^{-/-}$ mice. **(H)** Analysis of full-field electroretinography (ERG) for WT (n=8), *Prickle*$^{-/-}$ (n=5) or *Prickle3*$^{-/0}$ (n=5) mice. By dark-adaptation for a night, mice were analyzed for scotopic response and then photopic response. Data are mean± SEM of triplicates. * $P$<0.05, **$P$<0.01, *** $P$<0.001.